κ-Carrageenan/Sodium Alginate: A New Synthesis Route and Rapid Adsorbent for Hydroxychloroquine Drug

Mohammed Kassim Al-Hussainawy[1*] and Layth Sameer Al-Hayder[2]

[1]*Department of Chemistry, College of Education, University of Al-Qadisiyah, 58002 Diwaniya, Iraq*

[2]*Department of Chemistry, College of Education, University of Al-Qadisiyah, 58002 Al-Muthanna City, Iraq*

Abstract: *In recent years, the huge amounts of chemicals that are used as drugs and their derivatives have been exposed to the environment due to the COVID-19 pandemic. Some of these drugs (i.e. hydroxychloroquine (HCQ)) have a serious risk on aquatic media. In this study, carrageenan/sodium alginate (κC/Sa) was investigated as a biopolymer, environmentally friendly, and rapidly adsorbent to eliminate HCQ from its aqueous solution. The biopolymer (κC/Sa) was synthesized by free radical polymerization assisted by ultrasound in the presence of acrylic acid as cross-linkage and potassium persulfate as an initiator. The natural κC/Sa was characterized by FTIR, XRD, BET, BJH, and SEM techniques. The produced co-polymer had a mesoporous surface with high purity and significant thermal stability. The best parameters were determined to be 0.05 g biopolymer, 200 ppm initial HCQ concentration, salts, and pH = 7. The adsorption mechanism follows a pseudo second-order kinetic model, and the adsorption isotherm follows a Freundlich model, with q_e reaching 89.8 mg/g at 500 ppm HCQ. Thermodynamic studies indicated that the adsorption of hydroxychloroquine drugs was an exothermic spontaneous process.*

Keywords: *biopolymer; drug adsorption; pollution removal; hydroxychloroquine; κ-carrageenan/sodium alginate; aqueous media*

■ INTRODUCTION

Due to the extensive use of medicines, nutritional supplements, and other drugs in our daily lives, the removal of these substances from aqueous media has become a crucial environmental procedure in recent years [1-2]. Anticoagulants, analgesics, antibiotics, antidepressants, and anti-disease agents are based primarily on organic compounds with acid functional groups and amines linked to aromatic rings. They are intended for hospital, infirmary, and clinical pharmacy use. Their chemical structures are based primarily on organic compounds with acid functional groups and amines attached to aromatic rings [3-4]. One of these medicines, hydroxychloroquine (HCQ), is used in enormous amounts to treat a number of disorders (i.e., malaria and autoimmune diseases) all over the world [5]. One of the most frequently used antiviral medications in hospitals in recent months is hydroxychloroquine, which has received recommendations from numerous international organizations, including the FDA (World Health Organization), WHO, and the US Food and Drug Administration. This is particularly true given the coronavirus pandemic (SAR-CoV-2/COVID-19) and its recurrent use [6-7]. This medication's toxicity, chemical, and biological characteristics are only a few of its many drawbacks. Sadly, there are not many investigations into the elimination, oxidation, and fate (hydroxychloroquine in aqueous solution after use in different environments) of hydroxychloroquine in aqueous environments in the literature. Significant environmental contaminants include quinoline and its derivatives because of their persistence, carcinogenicity, and toxicity, even if the medicine is a quinoline derivative and the dangers to the environment remain unknown. Therefore, because of their high solubility and poor biodegradability, HCQ

and its derivative products both pose a risk to ecosystems and public health [8-9].

Among wastewater treatments are advanced oxidation processes (ultrasound degradation and photodegradation) and traditional methods (reverse osmosis, membrane separation, and adsorption). The adsorption process is the most effective, low-cost, and easily available method that has been successfully employed for removing pollutants from wastewater, so adsorption technology is critical to reduce adsorbates (dyes, medicines, organic compounds, factory, and hospital waste, etc.) because of rising environmental pollution and contaminants. Because biopolymers can achieve promising qualities and can be utilized again after filtration [10], we chose to employ them in our investigation, in particular for high molecular weight drugs and chemicals [11]. Numerous studies have focused on HCQ removal from aqueous solutions, such as through photodegradation [12], electrochemical oxidation [8], and gamma-irradiation [13]. On the other hand, there are many disadvantages to adsorbents. For example, clay has many disadvantages, such as pH-controlled adsorption, separating adsorbate-adsorbent mixture after adsorption, and it is not possible to regenerate the adsorbent through desorption. Although biomass in its natural state has been investigated as a potential adsorbent, its limited practical use is due to its low adsorption capability. The most popular adsorbent is activated carbon, although its use has been constrained by its expensive cost. Natural fibers are also expensive and can be shrunk after adsorption [11,14-15].

Brown algae can be used to extract the natural polymer sodium alginate. Outstanding qualities of sodium alginate include its great biocompatibility, biodegradability, and capacity for regeneration. Furthermore, carboxyl and hydroxyl groups that are plentiful have a strong adsorption affinity. However, sodium alginate has relatively low mechanical strength, stability, and heat resistance [16-18]. Therefore, to improve their suitability for adsorption, physical or chemical changes are typically used. Surface grafting, cross-linking, and compounding with other components have been used to modify sodium alginate-based adsorbents [19-20]. Additionally, combining alginate with other components can improve the chemical and physical adsorption properties of the composite. In order to change the physical and chemical characteristics of alginates and boost their adsorption capacity, alginates' physical and chemical characteristics were modified by carrageenan to enhance their adsorption ability [21-22]. Many academics have extensively researched how sodium alginate and carrageenan adhere to medicinal molecules [23-24]. This study aims to synthesize κ-Carrageenan/alginate hydrogel as an environmentally friendly and biodegradable adsorbent for the rapid adsorption of HCQ from its aqueous medium. Synthesis κ-Carrageenan/alginate hydrogel is a new method based on a closed glass tube in nitrogen and a water bath. The product was diagnosed by thermal and morphological measurements.

■ EXPERIMENTAL SECTION

Materials

Hydroxychloroquine (HCQ) was assayed at 98.4% and was equipped with Sigma (Shanghai, China). Aladdin (Shanghai, China) supplied κ-Carrageenan (κC), sodium alginate (Sa) purity 98%, and zinc oxide (ZnO) purity 99.0%. Also, acrylic acid (AA) at 99.5%, *N,N'*-methylenebisacrylamide (96%), and potassium persulfate > 98.5% were purchased from Aladdin. Commercial suppliers Sigma-Aldrich (Germany) provided calcium chloride ($CaCl_2$) and sodium chloride (94–97%). ddH_2O stands for double-distilled water it was used to prepare all solutions.

Procedure

Calibration curve

Hydroxychloroquine sulfate concentrations over the range of 1–10 ppm were prepared. However, analysis was done using a 340 nm wavelength by UV-visible spectroscopy, as shown in Fig. 1. Standard curves were produced twice in order to determine the differences that appeared. The stock solution was stored at 25 °C and protected from light before use.
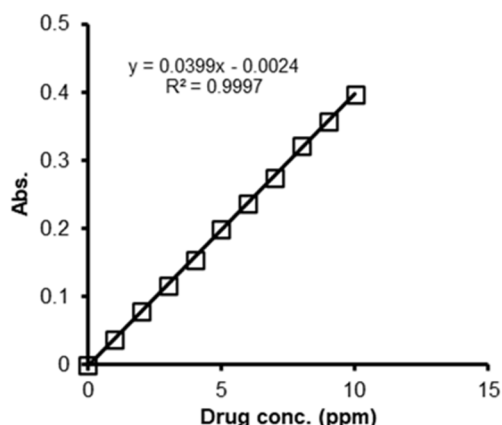
Fig 1. Calibration curve of HCQ drug

κC/Sa Dual hydrogel

The copolymer of κC/Sa hydrogel was prepared by solvating 1:1 w/w of carrageenan and alginate in double distilled water (ddH$_2$O) at a heat range (55–60 °C) for 25 min to form a κC/Sa solution in a homogenized shape with vigorous stirring until a vortex forms. The cross-linked 50 mg (*N,N'*-methylenebisacrylamide), 10 mg of initiator potassium persulfate (KPS), and 5 mL of acrylic acid (AA) were added to the homogenous solution (κC/Sa). These solutions were poured into glass tubes [25]. After that, the ultrasound is used to remove bubbles and the sample is placed in a water bath to complete the polymerization process. Finally, the prepared copolymer was washed with ddH$_2$O and dried at 65 °C in the oven. The κC/Sa hydrogel rocks were ground into tiny bits and sieved through a sieve with a mesh size of 150 mesh. The synthesis process is illustrated in Fig. 2 [26].

Characterization of κC/Sa hydrogel

The amorphous content of the κC/Sa adsorbent hydrogel was characterized by XRD using (XRD-6000, Shimadzu, Japan), and the radiation by CuKα (0.15040 nm). The XRD pattern was recorded in the range of 10°–80°. To determine the functional groups, spectra of the κC/Sa adsorbent hydrogel were performed using FTIR (Shimadzu, Japan, 8400 s). The morphology of the κC/Sa adsorbent hydrogel was observed by SEM (Scanning Electron Microscope) (MIRA3, Tescan, Czech Republic, Iran) with a voltage of 25 kV. The average pore
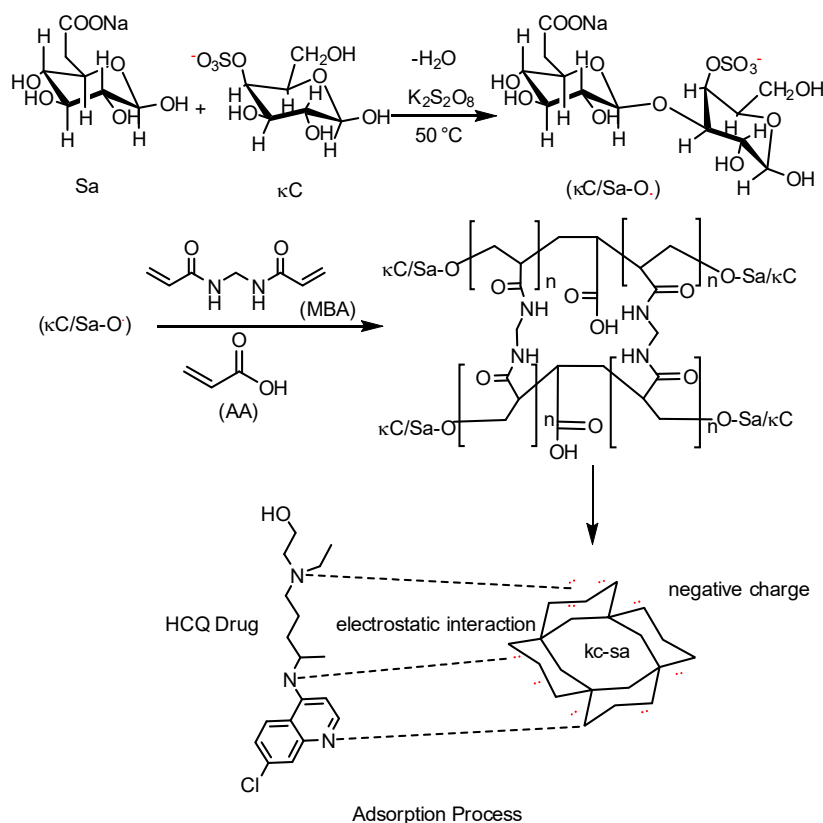
Fig 2. Mechanism of HCQ adsorption by active sites of alginate/carrageenan hydrogel

Mohammed Kassim Al-Hussainawy and Layth Sameer Al-Hayder

diameter and pore volume were observed by BET-BJH analysis (NOVA 2200e/Quantachrome/USA) of the κC/Sa hydrogel. The UV-1800 UV/Visible Scanning Spectrophotometer was performed using Shimadzu (Japan), and the thermogravimetric analysis (TGA, DTA) was done using Perkin Elmer (USA) (TGA 4000).

Protocol of adsorption

All adsorption tests were carried out in 50 mL cube tubes by combining and stirring 10 mL of an aqueous solution contaminated with HCQ with 50 mg of a hydrogel. The solution was centrifuged at 150 rpm after the recommended amount of contact time and filtered. Shaking 50 mg of hydrogel with 10 mL of HCQ solution at an initial pH of 7 and a temperature of 25 °C for varied contact periods between 1 and 180 min was used to conduct adsorption kinetics studies in flasks. By mixing 50 mg of hydrogel with 10 mL of HCQ solution in a 50 mL cube tube and adjusting the temperature from 10 °C to 40 °C, isotherm and thermodynamic parameter tests were also carried out. With a maximum wavelength of 340 nm, a UV-Vis spectrophotometer was used to measure residual HCQ concentrations [27]. Equations were used to determine the quantity of adsorbed HCQ per gram of adsorbent at equilibrium.

$$q_e = \frac{C_0 - C_e}{X} \tag{1}$$

$$R\% = \frac{C_0 - C_e}{C_0} \times 100 \tag{2}$$

where, q_e = Amount of drug adsorbed per unit mass of adsorbent (mg/g), C_0 = Initial drug concentration (mg/L), C_e = Final drug concentration (mg/L), X = Dose of adsorbent (g/L), and R% = removal percentage of dye.

Equilibration time for adsorption

Hydroxychloroquine was done with 50 mg of κC/Sa hydrogel in a 10 mL solution at a 200 ppm concentration. For periods of 1, 2, 4, 6, 10, 15, 30, 45, 60, 90, 120, and 180 min, separate tubes were equilibrated. The samples were separated by filtered paper after each equilibration period, and the HCQ content in the supernatant was calculated by comparing them to the standard curve using UV/vis spectrophotometry at 340 nm.

■ RESULTS AND DISCUSSION

Adsorbent Characterization

FTIR analysis

The FTIR spectra of the κC/Sa hydrogel before adsorption in the 4000–400 cm^{-1} wavelength range are displayed in Fig. 3. The OH absorption vibration peak at 3440–3150 cm^{-1} is due to the overlapping that occurred between the two O–H bands of the carboxyl and hydroxyl groups and the N–H group of the MBA crosslinker; the peaks at 1044 cm^{-1} correspond to glycosidic linkage; a peak formed at 1719 cm^{-1} can be attributed to the carbonyl group. The characteristic peak at 1455 cm^{-1} is caused by the symmetric stretching of the COOH groups. Peaks (S=O) appear at 1250 cm^{-1} and 2680 cm^{-1}, which correspond to CH asymmetric stretch [28-29]. The retention of carrageenan and sodium alginate's distinctive absorption peaks in the κC/Sa hydrogel demonstrated
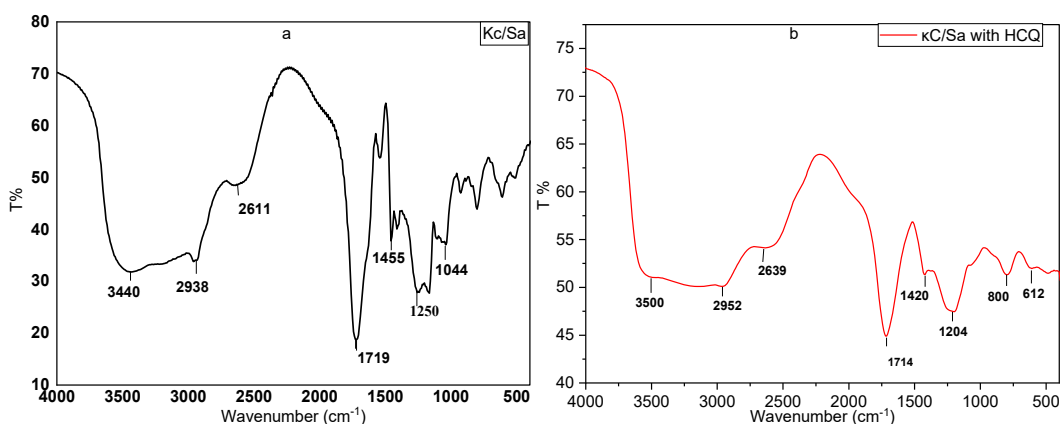
Fig 3. FTIR of κC/Sa hydrogel: (a) before adsorption, (b) after adsorption

Table 1. FTIR of κC/Sa hydrogel: (a) before adsorption, (b) after adsorption

Assignment group	a	b
ν(O–H, N–H) Overlapping	3440–3000	3000–3500
ν(C–H) Symmetric	2938	2952
ν(C–H) Asymmetric	2680	2639
ν(CO₃)	-	-
ν(C=O)(–COOH) and (–CONH)	1540–1719	1714
ν(C–N)	1395	1420
ν(S=O)	1180–1250	1204
ν(C–O–C)	1044	-
ν(OH) Wag	612	612

that the final result was a composite biopolymer containing both substances. The various functional groups on the surface, including the hydroxyl, carboxyl, and amino groups, have a significant impact on the adsorption of HCQ medication from an aqueous solution by κC/Sa hydrogel. Upon protonation and deprotonation, hydrogel functional groups' surfaces may become charged (negative and positive) or neutral. The FTIR spectral data shown in Fig. 3 supports the different interactions between the adsorbent and adsorbate, including electrostatic attractions and hydrogen bonding interactions, which are supported by the FTIR spectral data. Additionally, after HCQ drug adsorption, a broadband of 3400 cm^{-1} was moved to a higher wavenumber of 3500 cm^{-1} due to the weakened κC/Sa wavenumber of intermolecular hydrogen bonding between its molecules [30].

Specific surface area "BET and BJH"

According to the BET analysis, the composite hydrogel possesses a microporous structure. Simultaneous BJH analysis revealed the surface to have a mesoporous structure. The microporous limit is, however, quite near 437.44 and 46.13 in the BET-BJH analysis, as shown in Table 2. The pores visible in the SEM pictures confirm the BET-BJH analysis' findings. One of the crucial metrics to describe the adsorbents' quality is their surface area and pore size. Table 2 displays the BET-BJH specific surface area, pore size, and overall pore volume of κC/Sa adsorbed hydrogels. The majority of κC/Sa adsorption hydrogels have a microporous structure. Fig. 4 displays the nitrogen gas adsorption-desorption isotherms of κC/Sa adsorbed hydrogels. It was discovered that the BET-BJH isotherms had a relatively

Table 2. Results of the κC/Sa adsorbent hydrogel's of BET-BJH analysis

	Surface area (m²/g)	Average pore size (nm)	Pore volume (cm³/g)
BET	0.17442	437.44	0.019075
BJH	2.1088	46.13	0.013739
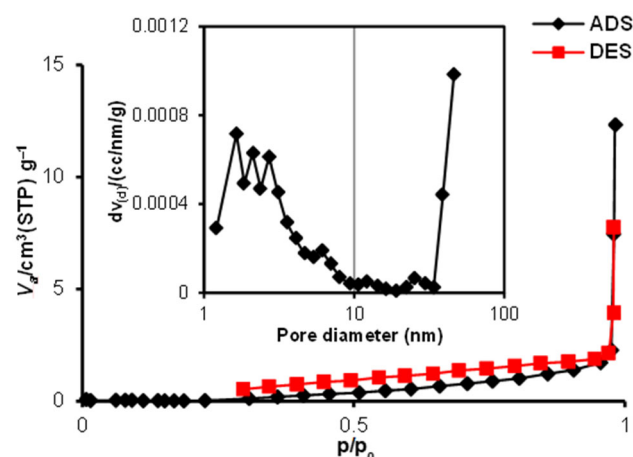
Fig 4. Adsorption-desorption isotherms and pore size distribution (inset) for the κC/Sa adsorbent hydrogel

large surface area. It is the adsorbate uptake grows exponentially in type III isotherms of κC/Sa because of the weak contact between the adsorbate (N₂ gas) and the adsorbent isotherm. The isotherm in Fig. 4 displays the H3 hysteresis loop, which denotes the presence of micropores [31]. The BJH result indicated that the surface has two different types of pores; mesopores (diameter 2–50 nm) and micropores (diameter < 2 nm).

XRD analysis

In Fig. 5, the XRD patterns for κC/Sa are displayed. The single broad peak in Fig. 5 at 2 of 21.1068 indicates

that κC/Sa is semicrystalline in nature with a high concentration of amorphous material. Two peaks in the XRD pattern of κC/Sa indicate semi-crystallinity: one at 21.1068°, which pertains to a hydrated crystalline structure, and the other at 37.7643°, which is related to an amorphous state [32]. Table 3 shows the XRD analysis results of the κC/Sa hydrogel.

SEM characterization

The cross-linked κC/Sa composite hydrogels feature rough surfaces and many folds and are well cross-linked, as shown in the SEM images shown in Fig. 6. These characteristics are crucial for improving the availability of more adsorption sites and a specified surface area for drug pollutants. Adsorbents' adsorption qualities are significantly influenced by their structure and surface characteristics. Additionally, the properties of the contaminants affect how the adsorbents and pollutants interact. In general, surface characteristics of adsorbents have the greatest impact on physical adsorption, whereas surface functional groups have the greatest impact on chemical adsorption.

In addition, alginate/carrageenan utilizing energy dispersive EDX [33] spectroscopy was further studied (Fig. 7). A mixed display of C, O, and S signals the presence of S
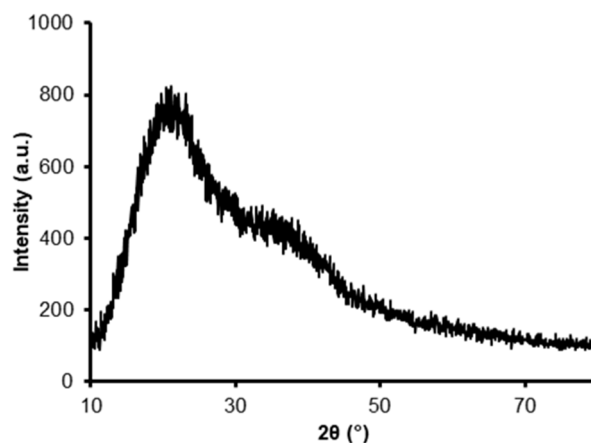
Fig 5. XRD patterns of κC/Sa hydrogel
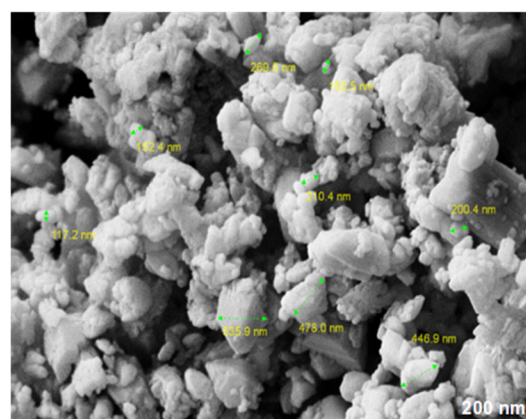
Fig 6. SEM image of κC/Sa hydrogel

Table 3. XRD analysis results of κC/Sa adsorbent hydrogel

Position 2θ (°)	Height (cts)	FWHM left 2θ (°)	d-spacing	Rel. int. (%)	Tip width	D (nm)
21.1068	446.61	0.1476	4.20927	96.10	0.1771	55.266
37.7643	41.64	0.1476	2.32303	8.96	0.1771	53.19
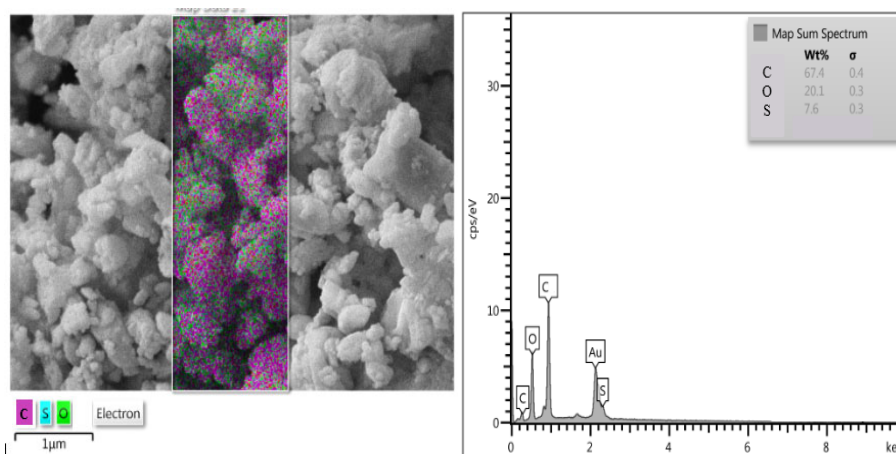
Fig 7. EDX map of composite of κC/Sa hydrogel
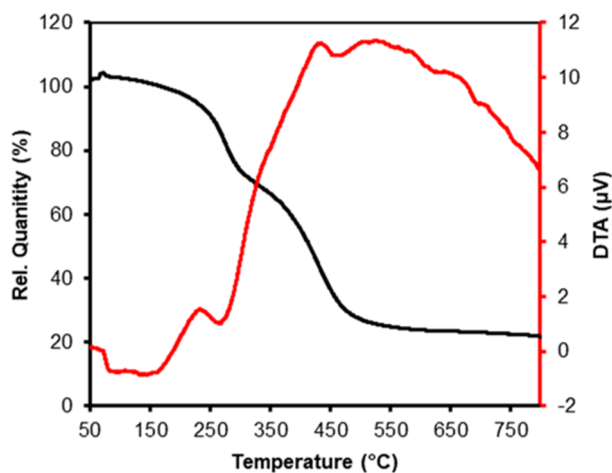
Fig 8. Thermogravimetric analysis (TGA/DTG) of κC/Sa hydrogel

of the sulfate ion. However, C is derived from natural polymers, and S is derived from potassium persulfate, which is used as an initiator [34].

Thermogravimetric analysis (TGA/DTG)

The relative stability of hydrogels could be evaluated by thermogravimetric analysis, and to demonstrate the purity of the produced hydrogels, thermogravimetric analysis of the κC/Sa hydrogel was carried out throughout a temperature range at a heating rate of 2 °C/min from 30 °C to 820 °C. The TGA curve (Fig. 8) shows three stages of weight loss, the first in the range of 5% weight loss at 110–200 °C involving evaporation of free water in the porous hydrogel. The second weight loss of 28% was observed at the temperature range of 200–300 °C, indicating the temperature corresponding to 10% weight loss of polymer as a result of thermal degradation of κC/Sa hydrogel. The last stage of weight loss was the κC/Sa polymer structural decomposition observed over the range of (320–500°).

DTA curves show four endothermic peaks at 150, 425, 500, and 650 °C, the first peak explains the physical water loss. The endothermic peaks located between 425 and 650 °C have been assigned to different stages of thermal hydrogel degradation [35-36].

Adsorption Properties of κC/Sa Hydrogel

For batch HCQ adsorption experiments, place 0.05 g of sorbent in a 10 mL batch bottle at pH 7.4 and temperature 25 °C. The concentration of hydroxychloroquine solution was 200 ppm in adsorption kinetic experiments and 50–500 mg/L in adsorption isotherm experiments. In the investigation, the greatest adsorption capacity of κC/Sa biopolymer to HCQ drug reached 89 mg/g, and the adsorption reached a situation of equilibrium after about 1 h.

Fig. 9(a) and 9(b) depict, respectively, how pH and the concentrations of $CaCl_2$ and NaCl affect the adsorption of HCQ on κC/Sa hydrogels using 0.1 mol/L of NaOH and HCl. The pH was changed from 2 to 11. The pH serves as the basis for determining the substance's adsorption on the surface of the gel since it affects the form in which HCQ is present [36]. Fig. 9(d) shows the influence of the contact time on the removal percentage of HCQ on κC/Sa hydrogel at natural pH of 25 °C. As presented in Fig. 9(c), the adsorption of κC/Sa hydrogel on HCQ increased with the drug's starting concentration at various temperatures. Based on the evaluation of the experimental results, at pH 4–9, the κC/Sa hydrogel is comparatively stable. The adsorption capacity reached a maximum of 89 mg/g at pH 8. This is because HCQ is most commonly in cationic form at pH 7–8. The hydrogel's zeta potential research reveals that it is negatively charged. Therefore, the κC/Sa hydrogel has a strong electrostatic adsorption capacity for HCQ under alkaline conditions [37-38]. During the adsorption process, when adding different concentrations of NaCl and $CaCl_2$ (0.001, 0.005, 0.01, 0.05, 0.1, and 0.15 mg/L^{-1}), adsorption capacity can be significantly impacted by ionic strength by managing electrostatic interactions during the process [39]. The equilibrium adsorption capacity was only 26.1 mg/g when the ionic strength was 0.15 mg/L^{-1}, as shown in Fig. 9(b), whereas the adsorption capacities for NaCl and $CaCl_2$ were 34.1–34.4 at 0.001 mg/L^{-1}. This is because an increase in ionic strength may reduce electrostatic interaction by concealing the surface charge, which can be either attracting or repulsive [40-41]. Specifically, HCQ is prevented from reaching the surface of hydrogels by the competing adsorption of positively charged Na^+, Ca^{+2}, and HCQ particles.

To clarify the dynamics of adsorption of HCQ on κC/Sa hydrogels, two recognizable kinetic models (pseudo-first-order and pseudo-second-order models)
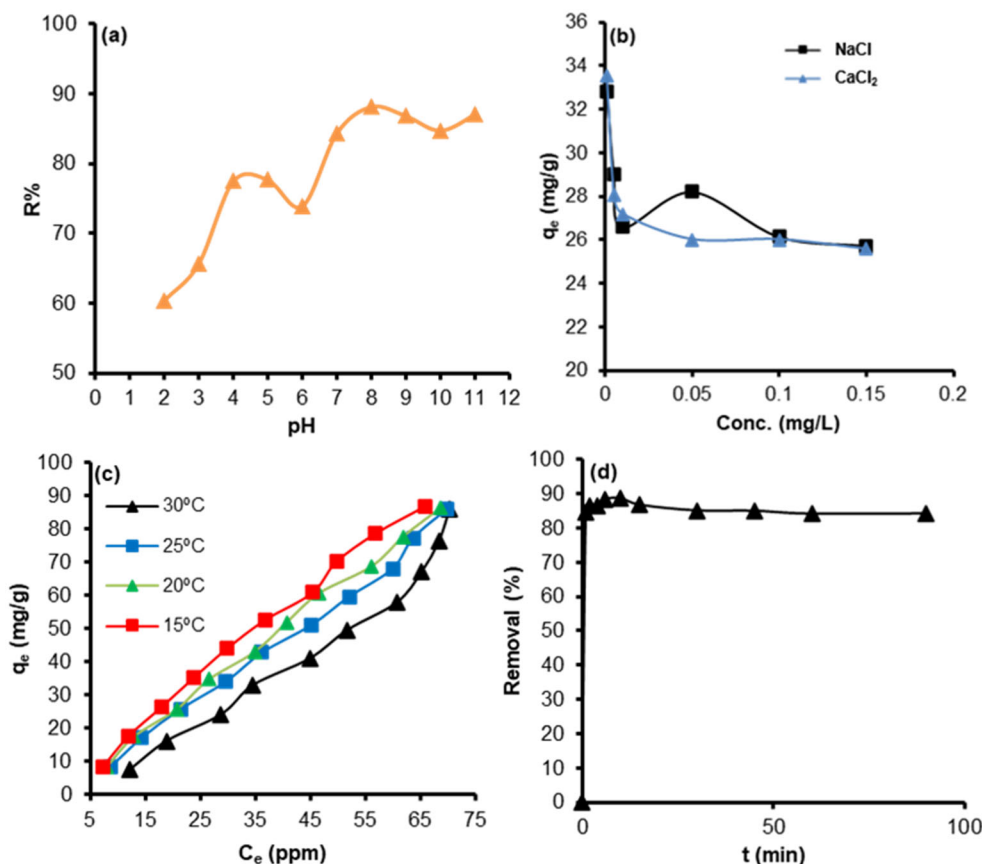
Fig 9. (a) Effects of pH on HCQ adsorption on κC/Sa hydrogel; (b) Influence of concentration of salts on HCQ adsorption; (c) Influence of temperature on HCQ adsorption (d) Influence of the contact period on the adsorption of HCQ on κC/Sa hydrogel

were used to survey the dynamic adsorption properties. Table 4 displays the parameters of the two kinetic models. The effect of contact time on the adsorption of κC/Sa the two kinetic models' parameters In Fig. 10(a), the effect of contact time on κC/Sa hydrogel adsorption hydrogel on HCQ is shown. Fig. 10(b) shows the fitted curves for different kinetic models. The pseudo-second-order and pseudo-first-order kinetic models displayed greater R^2 scores than the other models (Table 4), showing that the adsorption process is a heterogeneous diffusion process and that κC/Sa hydrogels contain several types of binding sites. There is contact between HCQ and the adsorbent, and near the border of the adsorbent particle, the adsorption resistance is concentrated [42]. It is discovered by fitting that the adsorption of κC/Sa hydrogel on HCQ is in good agreement with a more precise forecast of adsorption capacity is made when using a pseudo-second-

Table 4. Kinetic parameter of HCQ on κC/Sa hydrogel using two model

Model	Parameter	κC/Sa hydrogel
Pseudo-first-order	R^2	0.8708
	q_e ppm	2.6695
	K_1	0.0756
Pseudo-second-order	R^2	1
	q_e ppm	35.335689
	K_2	0.109711

order kinetic model and a correlation coefficient of 100%. Furthermore, the κC/Sa hydrogel was compared to earlier reported adsorbents for removing HCQ. As shown in Table 5, adsorption isotherm models are frequently used to symbolize the properties and mechanisms of the phases of liquid and solid during adsorption. The Langmuir [43] and Freundlich [44] isotherms are usually chosen to study the adsorption
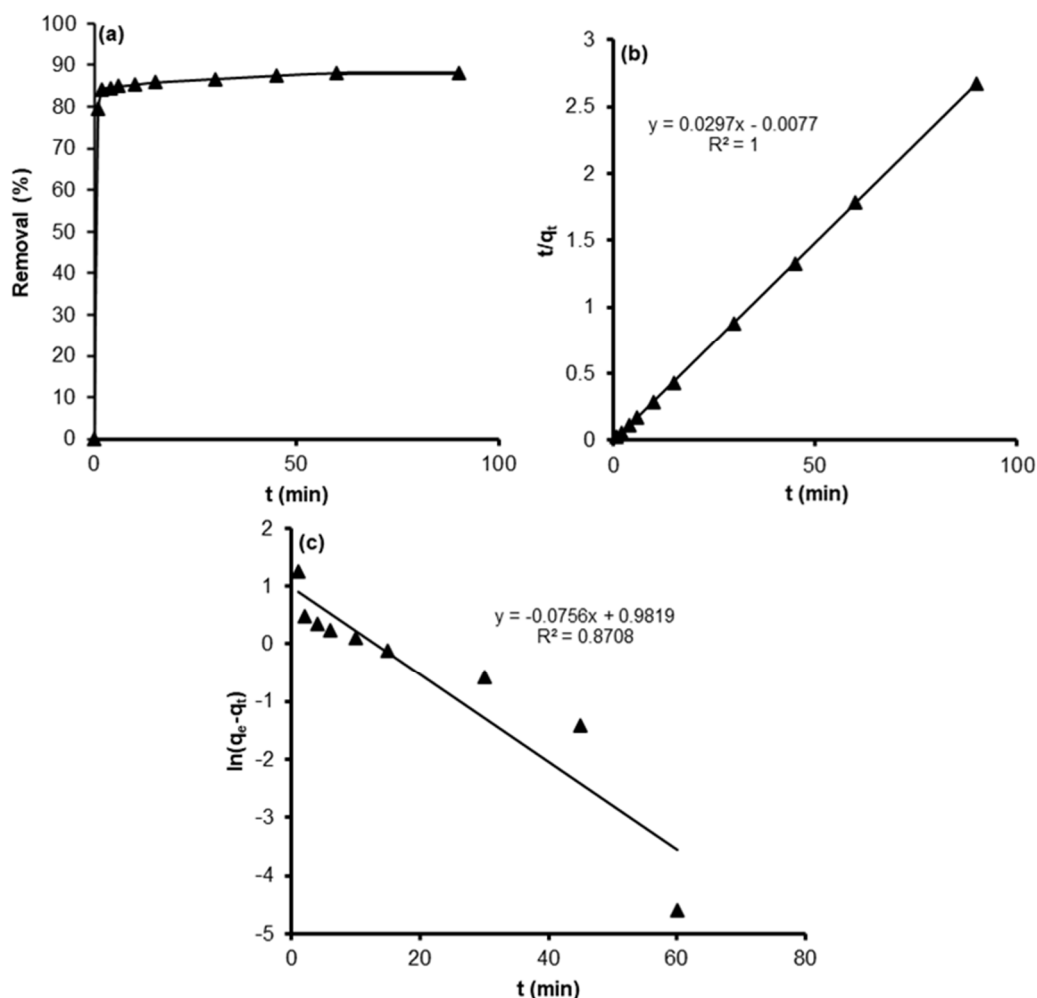
Fig 10. Kinetics curve: (a) κC/Sa hydrogel, and the adsorption kinetic model fitting graphs, (b) pseudo-second-order, (c) pseudo-first-order (adsorbent dosage): 0.05 g, HCQ: 10 mL and 200 mg/L)

Table 5. Isotherm parameters of HCQ adsorption on κC/Sa hydrogel using different models

Model	Parameter	κC/Sa hydrogel
Freundlich	k_F	1.32801
	n_F	0.984446
	R^2	0.9902
Temkin	B	35.556
	K_T	0.136709
	R^2	0.9463
Langmuir	q_m	625
	K_L	0.0025
	R^2	0.8131

attitude of HCQ on hydrogel. Fig. 11 a shows the adsorption isotherm of HCQ at the overfit.

It was found that the adsorption of κC/Sa hydrogel on HCQ was in good agreement with the pseudo-second-order kinetics, and the correlation coefficient was 100%. Three isotherm models (Freundlich, Langmuir, and Temkin models) were adopted for dataset fitting in order to better explain the adsorption process, as illustrated in Fig. 11. Table 4 displays the evaluation parameters for the model. The Langmuir model, however, cannot accurately predict the adsorption behavior of hydrogels in real-world studies [45], which should be attributed to the gel's structure and frequently misunderstood isotherm features. In the adsorption procedure itself, the gel adsorption data was found to best fit the Freundlich model based on the
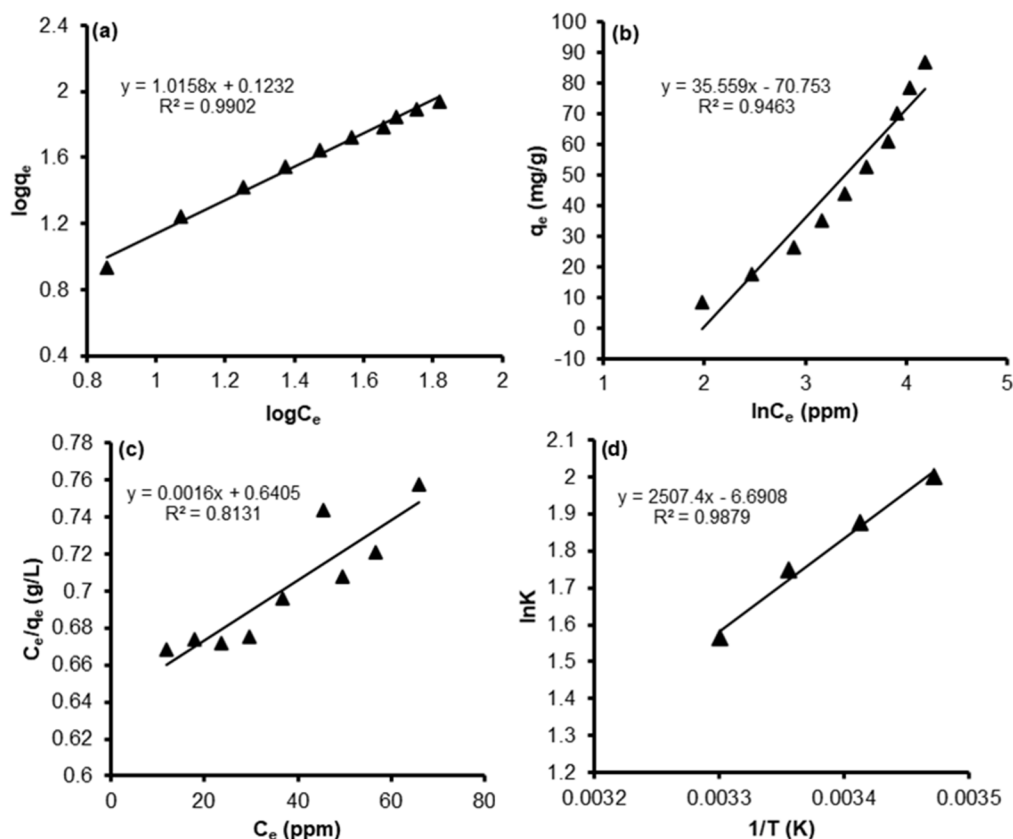
Fig 11. Adsorption isotherms on HCQ adsorption of κC/Sa hydrogel, graphical graphs showing the fits of various models for adsorption isotherms: (a) Freundlich, (b) Temkin, (c) Langmuir, (d) Van Hove plot of κC/Sa hydrogel

Table 6. Thermodynamic parameters of κC/Sa hydrogel

Temperature (K)	$\Delta G°$ (kJ mol^{-1})	$\Delta H°$ (kJ mol^{-1})	$\Delta S°$ (J mol^{-1})
288	-4.79126		
293	-4.57189	-20.8465	-55.4299
298	-4.32841		
303	-3.94154		

isotherm fitting results. Additionally, a good fit with the Freundlich model was attained, illuminating the gel's extremely uneven surface. These findings imply the existence of several adsorption sites in the κC/Sa hydrogel and the possibility of physical and chemical interactions between HCQ and the hydrogel [46-47]. Fig. 11(c) and 11(d) show the Temkin and Van Hove plots, respectively, of κC/Sa hydrogel, which explain the negative value of ΔH (-20.8465236 kJ mol^{-1}) as shown in Table 6, which indicates the exothermic nature of adsorption.

■ **CONCLUSION**

The polysaccharide-based hydrogel κC/Sa was prepared by cross-linking with *N,N′*-methylenebisacrylamide and exhibited high mechanical properties and excellent HCQ adsorption performance. It was found that due to the sulfate group (OSO$_3$) to Carrageenan molecule, κ-carrageenan can effectively improve the adsorption capacity of 500 ppm HCQ (89 mg/g) and the adsorption capacity of alginate/carrageenan composite gel for HCQ removal rate. The compressive strength and elasticity of Carrageenan composite gel can be successfully improved by sodium alginate, as well as its other mechanical characteristics. The combined gels' yield stress and storage modulus both dramatically increased. Carrageenan and sodium alginate's distinctive peaks remained in the FTIR spectrum, demonstrating that the

two materials were successfully bonded together. Because HCQ existed in various forms at various pHs, the results demonstrated that the pH of the solution had a significant impact on the adsorption process of the κC/Sa hydrogel. Additionally, the hydrogel's carboxyl groups have a significant function. This study shows better mechanical and adsorption characteristics of natural of biopolymer and offers a theoretical and practical foundation for the creation of alternative systems.

■ AUTHOR CONTRIBUTIONS

Mohammed Kassim Al-Hussainawy: performing simulation, methodology, data collection, conceptualization, investigation, formal analysis and visualization, writing (original draft), supervised. Layth Sameer Al-Hayder: formal analysis, visualization, investigation, writing (original draft), writing (review and editing), methodology, writing (review and editing), conceptualization, data collection. The whole manuscript was approved by all authors.

■ REFERENCES

[1] de Franco, M.A.E., de Carvalho, C.B., Bonetto, M.M., de Pelegrini Soares, R., and Féris, L.A., 2018, Diclofenac removal from water by adsorption using activated carbon in batch mode and fixed-bed column: Isotherms, thermodynamic study and breakthrough curves modeling, *J. Cleaner Prod.*, 181, 145–154.

[2] Babıć, S., Dabıć, D., and Ćurković, L., 2017, Fate of hydroxychloroquine in the aquatic environment, *Proceedings of the 15th International Conference on Environmental Science and Technology*, Rhodes, Greece.

[3] Kebede, T.G., Seroto, M.B., Chokwe, R.C., Dube, S., and Nindi, M.M., 2020, Adsorption of antiretroviral (ARVs) and related drugs from environmental wastewaters using nanofibers, *J. Environ. Chem. Eng.*, 8 (5), 104049.

[4] Parvinizadeh, F., and Daneshfar, A., 2019, Fabrication of a magnetic metal–organic framework molecularly imprinted polymer for extraction of anti-malaria agent hydroxychloroquine, *New J. Chem.*, 43 (22), 8508–8516.

[5] Nuri, E., Taraborelli, M., Andreoli, L., Tonello, M., Gerosa, M., Calligaro, A., Argolini, L.M., Kumar, R., Pengo, V., Meroni, P.L., Ruffatti, A., and Tincani, A., 2017, Long-term use of hydroxychloroquine reduces antiphospholipid antibodies levels in patients with primary antiphospholipid syndrome, *Immunol. Res.*, 65 (1), 17–24.

[6] Mahase, E., 2020, Covid-19: WHO halts hydroxychloroquine trial to review links with increased mortality risk, *BMJ*, 369, m2126.

[7] Li, X., Wang, Y., Agostinis, P., Rabson, A., Melino, G., Carafoli, E., Shi, Y., and Sun, E., 2020, Is hydroxychloroquine beneficial for COVID-19 patients?, *Cell Death Dis.*, 11 (7), 512.

[8] Bensalah, N., Midassi, S., Ahmad, M.I., and Bedoui, A., 2020, Degradation of hydroxychloroquine by electrochemical advanced oxidation processes, *Chem. Eng. J.*, 402, 126279.

[9] Gümüş, D., and Gümüş, F., 2022, Removal of hydroxychloroquine using engineered biochar from algal biodiesel industry waste: Characterization and design of experiment (DoE), *Arabian J. Sci. Eng.*, 47 (6), 7325–7334.

[10] Özçimen, D., İnan, B., Morkoç, O., and Efe, A., 2017, A review on algal biopolymers, *J. Chem. Eng. Res. Updates*, 4, 7–14.

[11] Jadhav, A.C., and Jadhav, N.C., 2021, "Treatment of textile wastewater using adsorption and adsorbents" in *Sustainable Technologies for Textile Wastewater Treatments*, Eds. Muthu, S.S., Woodhead Publishing, Sawston, United Kingdom, 235–273.

[12] Dabić, D., Babić, S., and Škorić, I., 2019, The role of photodegradation in the environmental fate of hydroxychloroquine, *Chemosphere*, 230, 268–277.

[13] Zaouak, A., Jebali, S., Chouchane, H., and Jelassi, H., 2022, Impact of gamma-irradiation on the

degradation and mineralization of hydroxychloroquine aqueous solutions, *Int. J. Environ. Sci. Technol.*, 2022, 1–10.

[14] Dias, J.M., Alvim-Ferraz, M.C.M., Almeida, M.F., Rivera-Utrilla, J., and Sánchez-Polo, M., 2007, Waste materials for activated carbon preparation and its use in aqueous-phase treatment: A review, *J. Environ. Manage.*, 85 (4), 833–846.

[15] Yadav, A., Bagotia, N., Sharma, A.K., and Kumar, S., 2021, Advances in decontamination of wastewater using biomass-basedcomposites: A critical review, *Sci. Total Environ.*, 784, 147108.

[16] Gao, X., Zhang, Y., and Zhao, Y., 2017, Biosorption and reduction of Au (III) to gold nanoparticles by thiourea modified alginate, *Carbohydr. Polym.*, 159, 108–115.

[17] Wang, S., Vincent, T., Faur, C., and Guibal, E., 2018, A comparison of palladium sorption using polyethylenimine impregnated alginate-based and carrageenan-based algal beads, *Appl. Sci.*, 8 (2), 264.

[18] Ates, B., Koytepe, S., Ulu, A., Gurses, C., and Thakur, V.K., 2020, Chemistry, structures, and advanced applications of nanocomposites from biorenewable resources, *Chem. Rev.*, 120 (17), 9304–9362.

[19] Thakur, S., Sharma, B., Verma, A., Chaudhary, J., Tamulevicius, S., and Thakur, V.K., 2018, Recent progress in sodium alginate based sustainable hydrogels for environmental applications, *J. Cleaner Prod.*, 198, 143–159.

[20] He, J., and Chen, J.P., 2014, A comprehensive review on biosorption of heavy metals by algal biomass: Materials, performances, chemistry, and modeling simulation tools, *Bioresour. Technol.*, 160, 67–78.

[21] Pan, L., Wang, Z., Zhao, X., and He, H., 2019, Efficient removal of lead and copper ions from water by enhanced strength-toughness alginate composite fibers, *Int. J. Biol. Macromol.*, 134, 223–229.

[22] Wen, R., Tu, B., Guo, X., Hao, X., Wu, X., and Tao, H., 2020, An ion release controlled Cr(VI) treatment agent: Nano zero-valent iron/carbon/alginate composite gel, *Int. J. Biol. Macromol.*, 146, 692–704.

[23] Shamsudin, M.S., Azha, S.F., Sellaoui, L., Badawi, M., Bonilla-Petriciolet, A., and Ismail, S., 2022, Performance and interactions of diclofenac adsorption using alginate/carbon-based films: Experimental investigation and statistical physics modelling, *Chem. Eng. J.*, 428, 131929.

[24] Yadav, S., Asthana, A., Singh, A.K., Chakraborty, R., Vidya, S.S., Susan, M.A.B.H., and Carabineiro, S.A.C., 2021, Adsorption of cationic dyes, drugs and metal from aqueous solutions using a polymer composite of magnetic/β-cyclodextrin/activated charcoal/Na alginate: Isotherm, kinetics and regeneration studies, *J. Hazard. Mater.*, 409, 124840.

[25] Mandal, B., and Ray, S.K., 2014, Swelling, diffusion, network parameters and adsorption properties of IPN hydrogel of chitosan and acrylic copolymer, *Mater. Sci. Eng., C*, 44, 132–143.

[26] Abate, G.Y., Alene, A.N., Habte, A.T., and Getahun, D.M., 2020, Adsorptive removal of malachite green dye from aqueous solution onto activated carbon of *Catha edulis* stem as a low cost bio-adsorbent, *Environ. Syst. Res.*, 9 (1), 29.

[27] Hosseini, S.M., Farmany, A., Alikhani, M.Y., Taheri, M., Asl, S.S., Alamian, S., and Arabestani, M.R., 2022, Co-delivery of doxycycline and hydroxychloroquine using CdTe-labeled solid lipid nanoparticles for treatment of acute and chronic brucellosis, *Front. Chem.*, 10, 890252.

[28] Abdala Díaz, R.T., Casas Arrojo, V., Arrojo Agudo, M.A., Cárdenas, C., Dobretsov, S., and Figueroa, F.L., 2019, Immunomodulatory and antioxidant activities of sulfated polysaccharides from *Laminaria ochroleuca*, *Porphyra umbilicalis*, and *Gelidium corneum*, *Mar. Biotechnol.*, 21 (4), 577–587.

[29] Thangeeswari, T., George, A.T., and Kumar, A.A., 2016, Optical properties and FTIR studies of cobalt doped ZnO nanoparticles by simple solution method, *Indian J. Sci. Technol.*, 9 (1), 1–4.

[30] Al-Hussainawy, M.K., Mehdi, Z.S., Jasim, K.K., Alshamsi, H.A., Saud, H.R., and Kyhoiesh, H.A.K., 2022, A single rapid route synthesis of magnetite/chitosan nanocomposite: Competitive study, *Results Chem.*, 4, 100567.

[31] Işık, B., and Uğraşkan, V., 2021, Adsorption of methylene blue on sodium alginate–flax seed ash beads: Isotherm, kinetic and thermodynamic studies, *Int. J. Biol. Macromol.*, 167, 1156–1167.

[32] Al-Taweel, S.S., Saud, H.R., Kadhum, A.A.H., and Takriff, M.S., 2019, The influence of titanium dioxide nanofiller ratio on morphology and surface properties of TiO_2/chitosan nanocomposite, *Results Phys.*, 13, 102296.

[33] Jebur, M.H., Albdere, E.A., Al-Hussainawy, M.K., and Alwan, S.H., 2022, Synthesis and characterization of new 1,3-oxazepine-4,7-dione compounds from 1,2-diaminobenzene, *Int. J. Health Sci.*, 6 (S4), 4578–4589.

[34] Smith, B.C., 2019, Organic nitrogen compounds V: Amine salts, *Spectroscopy*, 34 (9), 30–37.

[35] Nadeem, U., and Datta, M., 2014, Adsorption studies on zinc(II) ions on biopolymer composite beads of alginate-fly ash, *Eur. Chem. Bull.*, 3 (7), 682–691.

[36] Riyandari, B.A., Suherman, S., and Siswanta, D., 2018, The physico-mechanical properties and release kinetics of eugenol in chitosan-alginate polyelectrolyte complex films as active food packaging, *Indones. J. Chem.*, 18 (1), 82–91.

[37] Yu, F., Cui, T., Yang, C., Dai, X., and Ma, J., 2019, κ-Carrageenan/sodium alginate double-network hydrogel with enhanced mechanical properties, anti-swelling, and adsorption capacity, *Chemosphere*, 237, 124417.

[38] Gu, L., McClements, D.J., Li, J., Su, Y., Yang, Y., and Li, J., 2021, Formulation of alginate/carrageenan microgels to encapsulate, protect and release immunoglobulins: Egg Yolk IgY, *Food Hydrocolloids*, 112, 106349.

[39] El Badawy, A.M., Luxton, T.P., Silva, R.G., Scheckel, K.G., Suidan, M.T., and Tolaymat, T.M., 2010, Impact of environmental conditions (pH, ionic strength, and electrolyte type) on the surface charge and aggregation of silver nanoparticles suspensions, *Environ. Sci. Technol.*, 44 (4), 1260–1266.

[40] Gao, L., Wang, Y., Yan, T., Cui, L., Hu, L., Yan, L., Wei, Q., and Du, B., 2015, A novel magnetic polysaccharide–graphene oxide composite for removal of cationic dyes from aqueous solution, *New J. Chem.*, 39 (4), 2908–2916.

[41] Lei, C., Wen, F., Chen, J., Chen, W., Huang, Y., and Wang, B., 2021, Mussel-inspired synthesis of magnetic carboxymethyl chitosan aerogel for removal cationic and anionic dyes from aqueous solution, *Polymer*, 213, 123316.

[42] Tang, J., Huang, J., Tun, T., Liu, S., Hu, J., and Zhou, G., 2021, Cu(II) and Cd(II) capture using novel thermosensitive hydrogel microspheres: Adsorption behavior study and mechanism investigation, *J. Chem. Technol. Biotechnol.*, 96 (8), 2382–2389.

[43] Rahimi, R., Solimannejad, M., and Farghadani, M., 2021, Adsorption of chloroquine and hydroxychloroquine as potential drugs for SARS-CoV-2 infection on BC_3 nanosheets: A DFT study, *New J. Chem.*, 45 (38), 17976–17983.

[44] Chen, T., Da, T., and Ma, Y., 2021, Reasonable calculation of the thermodynamic parameters from adsorption equilibrium constant, *J. Mol. Liq.*, 322, 114980.

[45] Liao, Q., Rong, H., Zhao, M., Luo, H., Chu, Z., and Wang, R., 2022, Strong adsorption properties and mechanism of action with regard to tetracycline adsorption of double-network polyvinyl alcohol-copper alginate gel beads, *J. Hazard. Mater.*, 422, 126863.

[46] Wang, C.J., Li, Z., and Jiang, W.T., 2011, Adsorption of ciprofloxacin on 2:1 dioctahedral clay minerals, *Appl. Clay Sci.*, 53 (4), 723–728.

[47] Han, D., Zhao, H., Gao, L., Qin, Z., Ma, J., Han, Y., and Jiao, T., 2021, Preparation of carboxymethyl chitosan/phytic acid composite hydrogels for rapid dye adsorption in wastewater treatment, *Colloids Surf., A*, 628, 127355.